# Pole-to-Pole Moisture Conditions for the IGY

By VICTOR P. STARR [1]), JOSÉ P. PEIXOTO [2]) and ROBERT G. MCKEAN [1])

*Summary* – A study of the mean atmospheric humidity conditions on a planetary scale during the IGY covering the calendar year 1958 is presented. The fields of mean precipitable water content and of the zonal and meridional transports of water vapor are analyzed for the entire globe. Zonally averaged values of the various quantities at several levels are presented in tabular form and compared whenever possible with previous results or indirectly are analyzed on the basis of information obtained from different sources. The structure of these fields is studied and the corresponding implications for the general circulations of the atmosphere are discussed. Finally the zonal water balance for all the globe is discussed and its implications analyzed.

## *1. Introduction*

The present study constitutes a natural extension of the previous work done by a number of investigators in trying to acquire a better understanding of the overall atmospheric water balance and to find its relationship to the general circulation of the atmosphere on a planetary scale. The total pole-to-pole flux of water vapor in the atmosphere and the distribution of precipitable water are investigated for the IGY, using all available aerological data for the calender year 1958. Encouraged by previous results and by the considerable improvement of the world network of aerological stations during the IGY year 1958, the writers have extended the water vapor studies to include the Southern Hemisphere. Although the aerological network is not yet sufficiently dense over large oceanic areas and over certain other parts of the Southern Hemisphere for performing detailed studies of the behaviour of the atmosphere, it seemed, however, that the IGY data would be adequate and the best yet available for undertaking a study of water vapor covering the entire globe. In spite of some uncertainties in defining the fields over regions of the hemispheres lacking sufficient observations, provided certain care is used and certain precautions observed in the process of analysis, it became apparent that it would be reasonable to assume that the major features of the water vapor transport and distribution fields are fairly well represented in the study. In fact, in comparing the computed poleward transport of water vapor with the balance requirements of the general circulation of the atmosphere

[1]) Department of Meteorology, Massachusetts Institute of Technology, Cambridge, Mass. 02139, USA.

[2]) Department of Meteorology, Massachusetts Institute of Technology, Cambridge, Mass. and The University of Lisbon.

the agreement is remarkably good at most latitudes. Furthermore, the present world wide analysis depicts the main characteristic features of the analyses obtained in studies done by various authors on a regional and local scale and the results obtained agree quite well with certain climatological statistics obtained by independent means.

Studies for the entire Northern Hemisphere using actual winds at given levels were carried out by STARR and WHITE [25][3]) STARR and PEIXOTO [21], [22], [23], STARR, PEIXOTO, and LIVADAS [24], and PEIXOTO [13], [14] for the year 1950. On a regional basis, the transport of water vapor over North America was studied by BENTON and ESTOQUE [2] and RASMUSSON [17], [18], [19], among others. There have been similar studies for Europe by GRIGOR'EVA [4], [5], [6]; for Australia by HUTCHINGS [7]; for Africa by PEIXOTO and OBASI [16], etc. With the establishment of additional observing stations during the recent IGY period, even more extensive studies of the water vapor transport fields became possible. PEIXOTO and CRISI [15] treated the humidity conditions for the Northern Hemisphere.

In addition, a considerable number of investigations of atmospheric water vapor flux on a broad spectrum of scales have been made during the past year (1967).

The present work, in extending the investigation to the Southern Hemisphere, provides for the first time a global evaluation of the humidity conditions on a planetary scale. Following our previous approach, attention is confined to the long term statistical properties of the moisture fields, averaged with respect to time and thus considered as a representation of the ensemble of the time sequence of individual instantaneous fields of the corresponding quantities.

## *2. The data and its representativeness*

The basic data used in this study were aerological observations taken during the calendar year 1958 of the recent International Geophysical Year. An extensive coverage of about 450 selected weather stations provided representative data over the entire globe. Where a choice was possible, the most reliable and meteorologically significant stations were selected. In areas where observations were sparse, all available data were used. Figure 1 shows the locations of the stations, indicated by dots, used in the present investigation.

The primary stations used were the rawinsonde stations. The upper-air data for these primary stations were obtained on punched cards or magnetic tape, while the secondary ones were taken from IGY microcards. These reports were checked and then processed by electronic means. All rawinsonde data available for each primary station were used, such data for most stations being available at least once each day. A majority of stations provided two soundings a day, some three and even four. Statistical computations were based upon all the data available at each station. For the Northern Hemisphere stations the data handling and machine processing were

[3]) Numbers in brackets refer to References, pages 330/331.

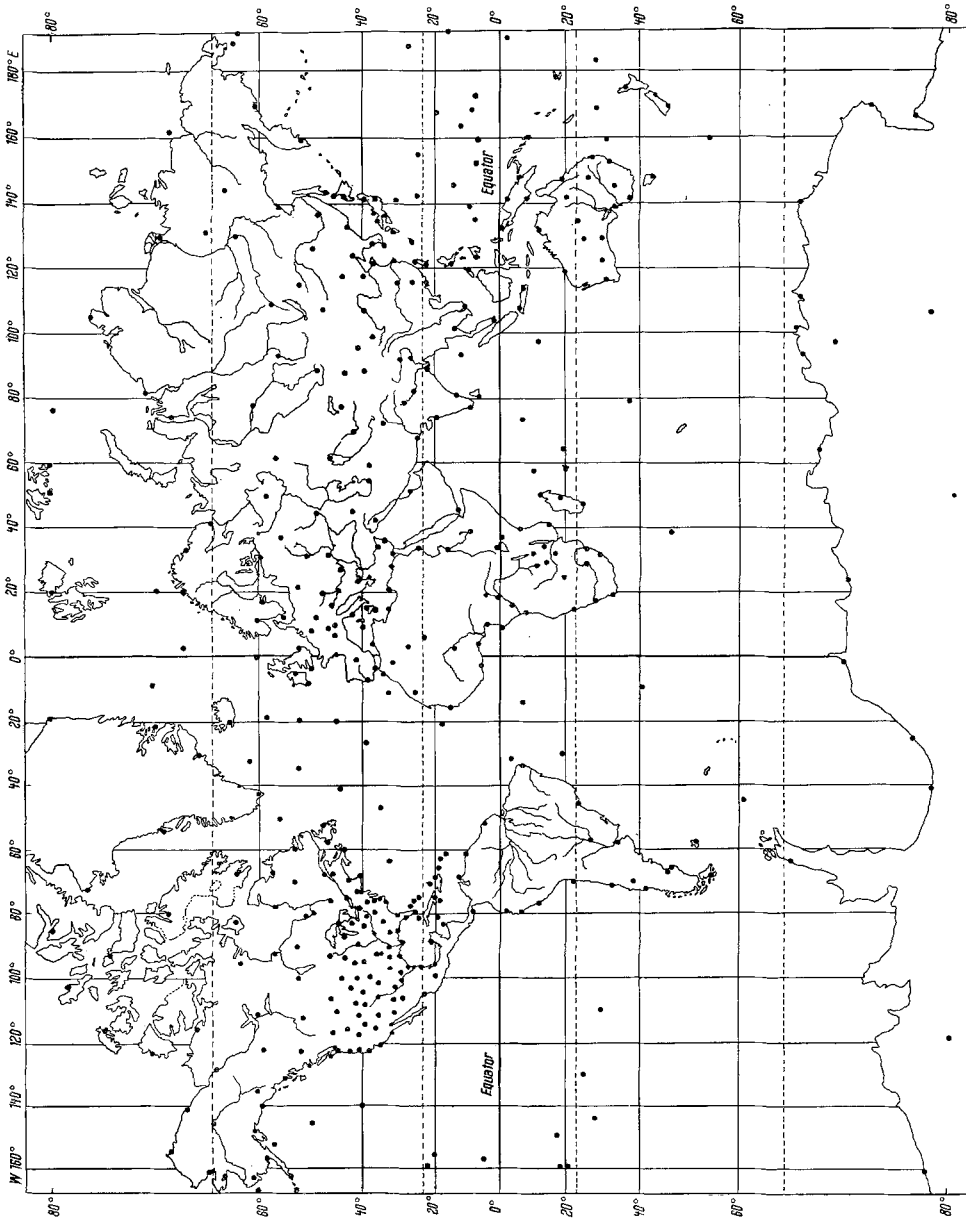


Figure 1 Distribution of the stations used in the investigation of the atmospheric water vapor conditions during the IGY

accomplished by the Air Weather Service Climatic Center, at Asheville, North Carolina, whereas for the Southern Hemisphere most of the computations were done by the M.I.T. Computation Center.

The secondary stations were used principally in critical areas not covered by the primary station network and also at a few stations chosen to fill in temporary gaps. The observations from these stations were obtained with either radiosonde, radiowind, pilot-balloon, rawinsonde procedures or a combination of these methods. The pilot balloon observations, as is well known, are not so reliable as those from the primary stations. These data were tabulated from the IGY microcards and were processed by the staff of the Planetary Circulations Project at M.I.T.

In spite of generally excellent coverage over the Northern Hemisphere, there were some areas with little or no data: the Amazon River Basin in South America, the eastern Pacific Ocean from Central America to the Hawaiian Islands, and the Indian Ocean. Nevertheless, the overall coverage of reliable data over the arctic and middle latitudes was excellent. The data from arctic stations were fairly complete north to 80 degrees latitude. The coverage over North America was especially dense over the United States; all stations in this area were used except a few deemed superfluous. The fair coverage over China, Mongolia, and especially the Tibetian plateau was most helpful.

When one views the surface of the Southern Hemisphere, perhaps the most noticeable characteristic is the large oceanic expanses, with relatively few land masses. Any contemplated atmospheric study of the Southern Hemisphere is hindered from the outset by the scarcity of observing stations for these areas. Wherever possible, island stations were used to improve the coverage over oceans, but a denser station network than now exists is really needed. Even over the continental land masses, there are large areas still uninhabited, such as Central Brazil and Antarctica. Fortunately, during the IGY several stations were maintained on the Antarctic continent. These stations combined to offer a fairly complete coverage for that region, including continual coverage of the South Pole itself (Amundsen-Scott Station). No stations were maintained over the interior of Brazil, however.

Wherever possible, supplementary data were used to improve the coverage. This included the addition of data from several stations maintained by the Australian government and not originally reported on the IGY cards due to irregular observation times. Data for the year 1958 were used exclusively, with the exception of Recife (82797) in Brazil and the Australian stations of Carnarvon (94300), Willis Island (94299), and Honiara (91517). Due to a scarcity of data for 1958 over Recife – only three months of observations were available – data from 1960 observations were substituted. In the case of the Australian stations, observations of specific humidity values were not available during 1958 and data for the years 1959, 1961, and 1962 were used for Carnarvon, Willis Island, and Honiara, respectively.

It is realized that the values of precipitable water and water vapor transport for these years are unlikely to be the same as for 1958, but the difference from one year

to the next should not perhaps be too large. In any event, it was felt that the use of values from a substitute year aids the final ana ysis and is more accurate than using no data at all over these regions.

Where possible, daily observations taken at 00Z were used, with observations for other times being used to fill gaps in the data. Actually, as with any statistical study, observations taken at random times should be included to avoid any possible bias due to diurnal variations. The irregular observation times for some Australian stations have already been mentioned. In the case of Gough Island (68906), 06Z observations were used exclusively, with the supplementary addition of some 12Z winds.

One final procedure was used to fill additional data gaps. Several pilot balloon stations were maintained at strategic points during the IGY, which reported daily winds. Using the analysis of specific humidity values reported by radiosonde and rawinsonde stations, a mean water content value read from the analyzed maps was assumed at each pressure level for these stations. These specific humidity values were then used in conjunction with the reported mean winds at each level, to obtain a measure of the transport at various pressure levels. The results were then integrated vertically to obtain an approximate measure of the net water vapor transport over each of the pilot balloon stations.

The mean values for specific humidity can be estimated rather accurately, since the distribution of the specific humidity field is primarily zonal. There is the disadvantage to this procedure, however, that it neglects the transport of water vapor due to transient eddies; but in the tropics and the equatorial zone where the winds are steady, this procedure should be expected to approximate the actual transport of water vapor somewhat accurately. In some cases (Pascua Islands, Pitcairn Island) the moisture fields were estimated using the data read off from daily analyzed maps for the International Geophysical Year published by the Weather Bureau of South Africa [27] by the Deutscher Wetterdienst [28].

In the interior of Brazil (Amazon region) estimates of water vapor content were obtained using surface observations. The upper air values were inferred by comparison with similar data for stations in other parts of the world with similar climates (e.g. parts of India in the south-west monsoon).

Data from four pressure levels were chosen for the study: the surface, 850 mb, 700 mb, and 500 mb. For some stations, 1000 mb data were used in place of the surface level observations. Since practically all the water content of the atmosphere is below 500 mb, no values were used from higher levels. Only the transport of water in the vapor phase was considered, since the transport of the liquid and solid phases is known to be small in comparison with the vapor phase (PEIXOTO [13]). It appears that the use of different types of radiosondes with different time lags for the humidity measurements does not affect substantially the mean conditions for a long period of time. The use of pilot-balloon stations introduces some bias in the moisture flux due to the missing reports in times of high cloudiness and high wind velocities, which may

lead to a slight underestimate of the magnitude of the transport, as the cloudiness is more predominant in air masses containing much moisture.

For some types of radiosondes the sensitivity of the humidity element is occasionally affected by the air temperature in regions where this falls below a critical value and the humidity is too low. This instrumental phenomenon known as 'motorboating' is most common in the upper levels of the dry regions. In our study when these conditions occurred the dew point temperatures were assumed to have the maximum possible values compatible with the observed temperature. This probably leads to an underestimate of the poleward flux since 'motorboating' conditions occur more frequently in the currents from the poles.

There are uncertainties inherent in the inaccuracies of the basic data and also portions of the computational procedures may introduce errors in the estimates of the various derived fields. Some aspects of these problems have been discussed among others by PEIXOTO [13], NYBERG [10], RASMUSSON [17], and others. Although these are very important sources of uncertainty when dealing with studies pinpointed in time and space, it seems safe to accept that for studies of large scale and embracing long periods of time such as the present one, the accuracy of the data is sufficient to depict the main characteristics of the water vapor flux in the atmosphere. By far, the bulk of the water content in the atmosphere and most of its flux occur below the 400 mb level where the upper air observations as obtained by classical methods are more abundant and the reliability of the instrumentation is better and the differences between individual systems less significant. Furthermore, for each radiosonde type, methods for minimizing the humidity time lag have been widely applied. Thus it seems that the vertical measurements in the lower atmosphere are fairly adequate for our present needs.

## 3. *Procedures*

The basic quantities used in this study are the specific humidity, $q$, the eastward wind component, $u$, and the northward component, $v$, the total horizontal wind vector being $\vec{v} = u\,\vec{i}_\lambda + v\,\vec{i}_\phi$.

Since the formulation of the problem and the methodology of the computation have been presented and discussed on several occasions by the writers, it seems sufficient to give only a general review of the approach followed.

The atmosphere may be considered in a state of hydrostatic equilibrium, so that the pressure may be taken as the vertical coordinate. A coordinate system $(\lambda, \phi, p, t)$ is used in which $\lambda$ denotes longitude, $\phi$ latitude, $p$ pressure and $t$ time. At a given isobaric level the mean horizontal transport field of water vapor in the time interval $\tau$ is represented by

$$\vec{F} = \frac{1}{g}\int_{\tau} g\,\vec{v}\,dt \tag{1}$$

where $g$ is the acceleration of gravity. Let us define the bar operator as a time average

for the time interval $\tau$,

$$\overline{(\ )} \equiv \frac{1}{\tau}\int_{\tau}(\ )\,dt. \tag{2}$$

It follows that the time average of $\vec{F}$ is given by

$$\overline{\vec{F}} = \frac{1}{g}\,\overline{q\,\vec{v}} = \frac{1}{g}\,(\overline{q\,u} + \overline{q\,v}) = \bar{F}_\lambda\,\vec{\imath}_\lambda + \bar{F}_\phi\,\vec{\imath}_\phi \tag{3}$$

where $F_\lambda = (1/g)\,q\,u$ denotes the zonal component and $F_\phi = (1/g)\,q\,v$ the meridional component of the horizontal vector field transport. The total horizontal transport of water vapor above a point on the earth's surface defines a two-dimensional vector field

$$\vec{Q} = \int_0^{p_0} \vec{F}\,dp = Q_\lambda\,\vec{\imath}_\lambda + Q_\phi\,\vec{\imath}_\phi \tag{4}$$

where $p_0$ represents the mean value of the surface pressure. The corresponding mean zonal and meridional components are then:

$$\bar{Q}_\lambda = \frac{1}{g}\int_0^{p_0} \overline{q\,u}\,dp \tag{5}$$

and

$$\bar{Q}_\phi = \frac{1}{g}\int_0^{p_0} \overline{q\,v}\,dp. \tag{6}$$

Similarly, the mean precipitable water content above a point on the earth's surface is expressed by

$$\bar{W} = \frac{1}{g}\int_0^{p_0} q\,dp. \tag{7}$$

For a unit column of air extending from the earth's surface (pressure $p_0$) at each point to the top of the atmosphere (pressure, $p=0$), the balance equation can be written, so that

$$\frac{\partial W}{\partial t} + \operatorname{div}\vec{Q} = \Sigma. \tag{8}$$

Here $\Sigma$ represents the net sources of water substance in the atmospheric column, and the other symbols have the customary significance. The main sources and sinks of water vapor in the atmosphere are due primarily to the evaporation $E$ at the surface of the earth and to precipitation $P$, since the condensation and the evaporation in

the clouds are of negligible importance because the solid and liquid water content in the clouds is very small. The advection of water in the solid or liquid phases is very small compared with the flux of water vapor in the atmosphere. Thus for all practical purposes $\Sigma$ is given by the excess of evaporation over precipitation, $(E-P)$. Thus, taking the time average for a given time interval (one year), the equation for atmospheric water vapor balance in the $(\lambda, \phi, p, t)$ coordinate system becomes

$$\frac{1}{R\cos\phi}\left[\frac{\partial \bar{Q}_\lambda}{\partial \lambda}+\frac{\partial}{\partial \phi}(\bar{Q}_\phi \cos\phi)=\overline{E-P}\right. . \tag{9}$$

Because of this time interval, $\partial \bar{W}/\partial t$ may be set to zero. The left-hand side of this equation, is the horizontal divergence of the total (vertically-integrated) yearly mean transport of water vapor in the atmosphere, $\operatorname{div}\bar{\bar{Q}}(\lambda, \phi)$.

STARR, PEIXOTO and LIVADAS [24] calculated the mean $\overline{(E-P)}$ field for a ten-degree, latitude-longitude grid over the northern hemisphere for the year 1950, using finite difference methods to compute the horizontal divergence of the water vapor transport. For a latitudinal belt bounded by the latitudes $\phi_1$ and $\phi_2$, equation (9) reduces to

$$\overline{[E-P]}=\frac{1}{2\pi[\sin\phi_2-\sin\phi_1]}\oint[(\bar{Q}_\phi\cos\phi)_{\phi_2}-(\bar{Q}_\phi\cos\phi)_{\phi_1}]\,d\lambda \tag{10}$$

since

$$\oint\frac{\partial Q_\lambda}{\partial\lambda}\,d\lambda=0\,.$$

Among other quantities, the yearly mean values $q$, $\sigma(q)$, $q\,u$, $q\,v$ were computed for each station at the four standard levels 1000, 850, 700 and 500 mb. The vertical integrations required to compute $W$, $Q_\lambda$ and $Q_\phi$ were performed numerically applying the trapezoidal rule. Whenever possible the actual mean surface pressure was used in evaluating the integrals. For those stations reporting values at 1000 mb rather than at the surface, the calculated integral will lead to an underestimate of the actual integral. It was found in previous studies that, with the exception of tropical areas, the contribution of the thin layer between 1000 mb and the surface was of little relative significance for the total integrated values. The largest differences probably occur over the trade wind regions, where low-level humidities are high, winds are strong, and the mean surface pressure exceeds 1000 mb. In cases where the mean surface pressure is less than 1000 mb or where the surface topography normally extends above the 1000 mb surface, the actual surface values of humidity and wind were used and substituted for the 1000 mb data; hence, no fictitious values were introduced into the vertical integrals for these cases.

Contributions to the vertical integrals were disregarded above 500 mb since the values of the specific humidity are, in general, small enough to be disregarded above that level over middle and high latitudes. However, these errors are likely to be

greater in the tropical and equatorial regions and over extensive areas of high terrain such as the Rocky Mountains, the Himalayas and the Tibet plateau region. An estimate of the error due to setting the upper boundary of vertical integrals at 500 mb, can be obtained if one assumes that the values of the various fields are negligible at 300 or at 200 mb. In fact, the contribution to the total vertical integrated value of water vapor transport in the layer between 500 and 300 mb ($\Delta p = 200$ mb) is given by

$$\bar{Q}_{\phi}^{500/300} \sim \frac{1}{g} \int_{300}^{500} \overline{q\, v}\, dp\,.$$

Assuming now that $\overline{q\, v} \sim 0$ at 300 mb, the contribution from the layer 500/300 mb to the total vertical integral is numerically given by $\bar{q}\, v\, 500/9.8$ or about 10% of the value of $\overline{q\, v}$ at 500 mb. In a typical case this might signify an error of perhaps 2% in evaluating the total integral.

Contributions to the vertical integrals from the higher levels have already been taken into consideration in studying the humidity conditions over Africa (PEIXOTO and OBASI [16]).

As a result of the foregoing assumptions in setting the boundary conditions for the vertical integrals, the magnitudes of the mean horizontal transport of water vapor $\vec{Q}$ and the mean precipitable water vapor content $\bar{W}$ were probably slightly underestimated; however, the underestimation was very likely confined chiefly to special areas of high terrain and to the trade wind regions. This small error approximates one percent of the value of $\bar{q}$ at 1000 mb in the case of $\bar{W}$.

In all computations, when 1000 mb, 850 mb, or 700 mb data were missing due to station elevation, as stated before, surface data were substituted for the missing level. The following elevation limits were used in selecting levels for the vertical integrals.

| *Station elevation* | *Levels used* |
|---|---|
| Sea level to 800 m. | 1000, 850, 700 and 500 mb with surface substituted if 1000 mb missing. |
| 800 to 2300 m. | 850, 700 and 500 mb with surface substituted if 850 mb missing. |
| Above 2300 m. | 700 and 500 mb with surface substituted if 700 mb missing. |

The yearly mean values of $\bar{q}$, $\overline{q\, u}$, $\overline{q\, v}$, $\bar{W}$, $\bar{Q}_{\lambda}$, and $Q_{\phi}$ for each station were plotted on separate charts and the corresponding fields were analyzed using standard procedures, on polar stereographic projection maps for both hemispheres and on mercator projection maps for the intertropical region. A variety of auxiliary charts were plotted and analyzed mainly over the intertropical region, in order to obtain additional information on the various quantities which are of interest for this study. With this

procedure the analyses of PEIXOTO and CRISI improved considerably mainly over the equatorial region. After having been adjusted the final analyses were transferred to the final globe mercator maps, as shown in the various figures of the present study. A five-degree latitude longitude grid was used to extract the corresponding grid point values, and finite difference methods were used for the computations needed. It was possible to evaluate numerically the mean zonal values of $\bar{W}$, $\bar{Q}_\lambda$, and $\bar{Q}_\phi$ defined as follows:

$$2\pi[\bar{W}] = \oint q \, d\lambda \tag{11}$$

$$2\pi[\bar{Q}_\lambda] = \oint \overline{q\,u} \, d\lambda \tag{12}$$

$$2\pi[\bar{Q}_\phi] = \oint \overline{q\,v} \, d\lambda \tag{13}$$

and also the equivalent values of $[\bar{q}]$, $[\sigma(q)]$, $[\overline{q\,u}]$, and $[\overline{q\,v}]$ at four isobaric levels.

## 4. *Analysis and interpretation of results*

### 4.1. *Mean precipitable water*

The field of the mean precipitable water vapor content, in the atmosphere, $\bar{W}$, is represented in Figure 2. The analysis did not involve major difficulties, since the data are quite sufficient and the patterns are relatively well defined. Isolines were drawn for every 0.5 gm cm$^{-2}$ of water vapor content. The analyzed $\bar{W}$ field shows, perhaps better than any other, the essentials of the water vapor distribution in the atmosphere. With few exceptions, the analysis shows a continuous decrease of precipitable water vapor content from the equator to the north and the south poles, which is to be expected since the ability of the atmosphere to retain water vapor is a function of the temperature and so the fields of $q$ and of $W$ are largely regulated by the temperature fields. As is well known, this is the basic reason why the relative humidity is to a degree a conservative property with respect to temperature changes (LORENZ, [8]).

The analysis shows the influence of oceans and continents on the distribution of the water vapor content in the atmosphere. On the whole the amount of precipitable water is higher over the oceans with the exception of the Amazon Basin, in general agreement with the results obtained by BANNON and STEELE [1]. The departures from zonal symmetry are clearly associated with the physiography of the globe. These effects are evident over both hemispheres. Looking at the northern hemisphere we see that the Sahara, the desert areas of the Middle East south of the Caspian Sea, and the desert region north of Tibet are dry. In addition, the effects of high terrain on moisture distribution are illustrated by the very dry areas (less than 1.0 gm cm$^{-2}$)

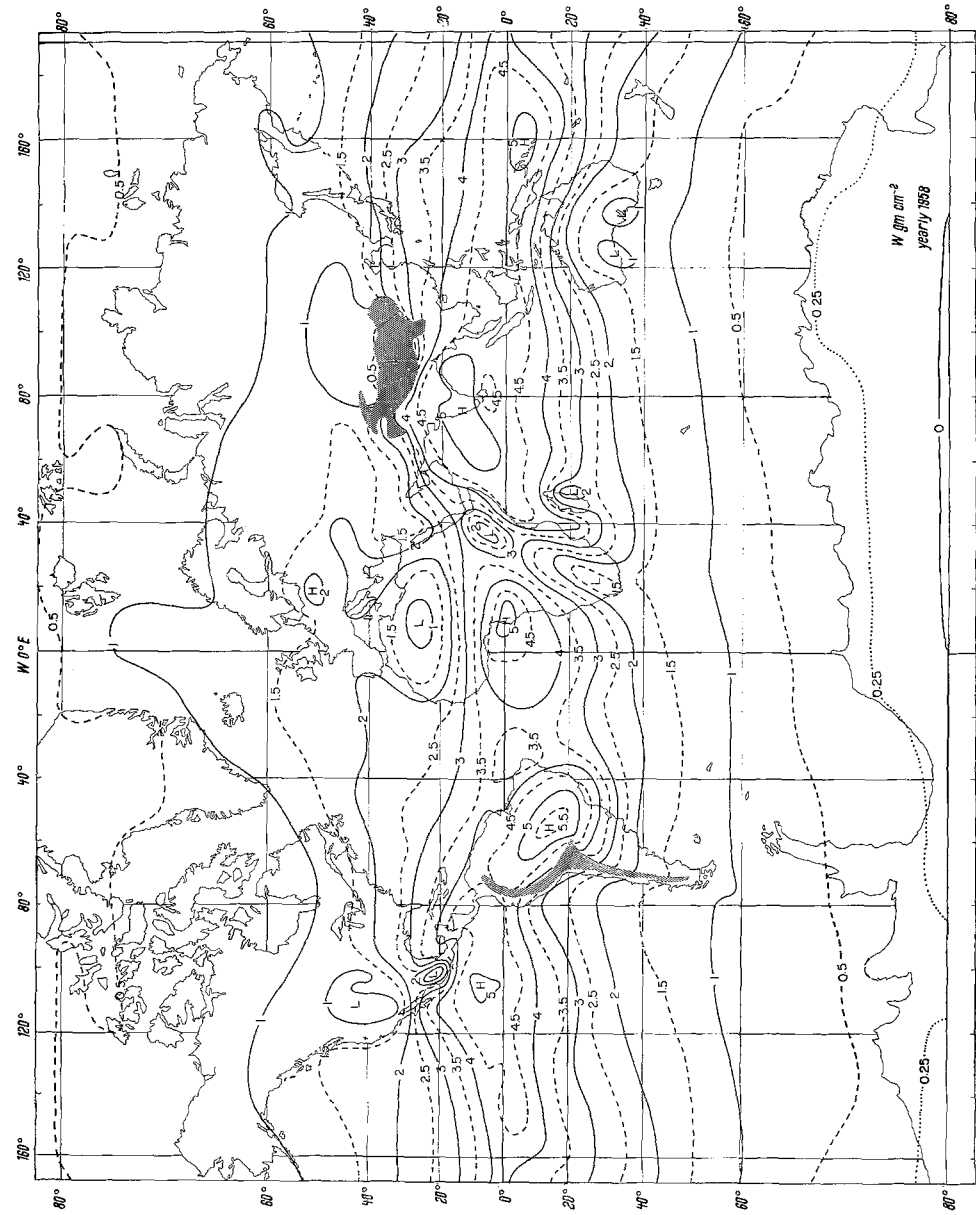


Figure 2. Time average of the vertically integrated values of specific humidity (precipitable water), $W$, in units of gm cm$^{-2}$ for yearly data. Isoline spacing (full curves) 1 gm cm$^{-2}$

over the Rockies in the western United States, over central Mexico, and over the Himalayan Mountains and plateaus of Tibet and Central Asia.

Over the western portions of the subtropical oceanic anticyclones in the northern hemisphere the water vapor content is generally higher than over the eastern portions; this fact is especially evident in the Pacific, and agrees with the concept of general convergence and divergence, respectively, in the western and eastern portions of these semi-permanent, large-scale features of the general circulation. The areas of highest water vapor content are the equatorial region of South America, the equatorial eastern and western Pacific Ocean, the Indian Ocean (especially south and east of India, including the Bay of Bengal) and equatorial West Africa. The driest area is in the Arctic, where the yearly mean precipitable water vapor content is less than 0.5 gm $cm^{-2}$ north of 80°N. The 1.0 gm $cm^{-2}$ isoline enclosing the Arctic regions is found generally at or near the latitude of 60°N; it dips south of 60°N over the regions of most frequent outbreaks of cold, dry polar continental air in eastern Siberia and the Bering Sea and eastern Canada and Hudson Bay; it extends north of 60°N and even slightly north of 70°N over Jan Mayen and northeast of Iceland, very probably showing the effects of the warm North Atlantic Drift current and warm, moist air masses frequently carried northeastward across the North Atlantic Ocean toward the Arctic Ocean. The 0.5 gm $cm^{-2}$ isoline encloses the area between 80°N and the north pole and also dips slightly southward toward eastern Siberia and over Greenland.

In the southern hemisphere, as illustrated in Figure 2, the distribution of precipitable water is practically zonal as anticipated. The largest values are in the equatorial regions, and there is a continuous decrease toward the south pole. There are a few exceptions to this zonal pattern, however, which merit comment.

The observed low center of precipitable water over central Australia is similar to that found by HUTCHINGS [7]. Its presence can be associated with the Great Victoria Desert of Australia and the corresponding dryness of that region.

Over the continent of Africa, there is a center of minimum precipitable water values over the central portion of the southern part of the continent, as observed by PEIXOTO and OBASI [16]. This is the region of the Kalahari Desert, and dry conditions are expected to prevail there.

The effects of topography are also evident over the Andes, the highlands of Ethiopia and the mountains of Kenya.

In general, the observed values of precipitable water for the southern hemisphere are slightly higher than the values for the northern hemisphere during the same period (PEIXOTO and CRISI, [15]). PEIXOTO and OBASI [16] likewise found higher values over southern Africa than over the northern part of that continent and attributed this to the effect of the trade winds. It now seems likely that higher mean temperature values for the southern hemisphere associated with a larger predominance of the oceans contribute to the higher observed values of precipitable water.

Using the grid point values from the map of $\bar{W}$, an estimate of the meridional

Table 1

*Meridional distribution of zonally averaged precipitable water vapor content* $[\bar{W}]$, *in grams per square centimeter for yearly data*

| Deg. Lat. | 0 | 5 | 10 | 15 | 20 | 25 | 30 | 35 | 40 | 45 | 50 | 55 | 60 | 65 | 70 | 75 | 80 |
|---|---|---|---|---|---|---|---|---|---|---|---|---|---|---|---|---|---|
| Northern Hemisphere | 4.39 | 4.31 | 3.99 | 3.63 | 3.11 | 2.78 | 2.18 | 1.83 | 1.64 | 1.47 | 1.32 | 1.19 | 1.04 | 0.89 | 0.70 | 0.58 | 0.48 |
| Southern Hemisphere | 4.39 | 4.37 | 4.09 | 3.70 | 3.25 | 2.77 | 2.32 | 1.95 | 1.70 | 1.45 | 1.21 | 1.00 | 0.72 | 0.51 | 0.36 | 0.25 | 0.12 |

distribution of zonally averaged precipitable water vapor content $\bar{W}$ was obtained. The resulting values are given in Table 1, and are also shown in Figure 3. The curve with the results obtained for the year 1950 by the writers is also included for comparison. The agreement is excellent, and so is the agreement over both hemispheres with the values published by SELLERS [20] obtained by independent means. As ex-

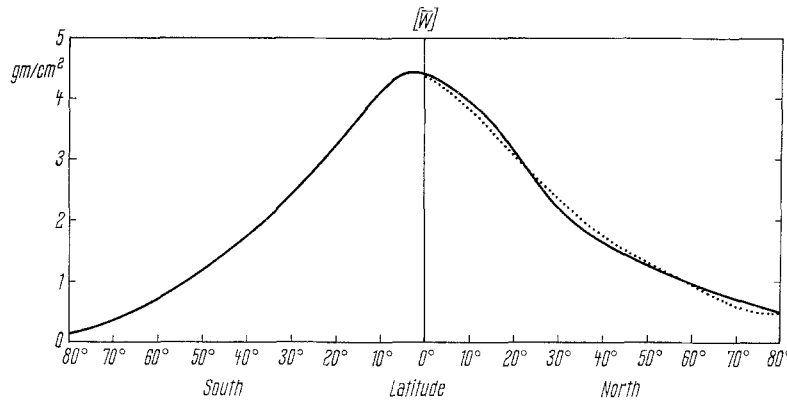


Figure 3
The meridional distribution of zonally averaged precipitable water vapor content computed from atmospheric data. The dotted curve represents the yearly distribution computed by Starr et al. for 1950. The units are gm cm$^{-2}$

pected the curve $\bar{W}$ shows a maximum slightly south of the equator and shows a continuous decrease from the equator to the poles ($\partial[\bar{W}]/\partial\phi < 0$) with the steepest gradient over the subtropical latitudes. The grand average precipitable water is of the order of 2.6 g/cm$^2$, with a slightly higher value over the southern hemisphere. It is then clear that the storage of the atmosphere for the water vapor is relatively small and the amount present could be completely removed by the average precipitation acting alone within a period of ten days (STARR *et al.* [23]). However, the total water vapor content for the entire atmosphere is still comparable to the water content in the rivers of the earth, as estimated by hydrologists. The distributions of the specific humidity and of its temporal standard deviation were also analyzed, but not reproduced in this paper. Nevertheless, in order to present some idea of the structure of the distribution of water vapor in the vertical and of its variability, the zonally averaged values of the specific humidity $[\bar{q}]$ and of its standard deviation $\sigma(q)$ were computed at various levels. The final results are given in Tables 2 and 3 and presented in Figures 4 and 5. The specific humidity decreases rapidly with latitude and height, with a strong vertical gradient in the lower layers of the atmosphere in the intertropical region. Inspection of Figure 4 shows immediately that about 50 percent of the water vapor is contained in the lowest 15 percent of the atmosphere, and nearly 90 percent in the lower half of the atmosphere. The gradient along the vertical is strongest within the tropical region and in the lower layers of the atmosphere. As is

Table 2

*Zonally averaged values of the mean specific humidity, $[\bar{q}]$, in grams per kilograms, for yearly data*

| Deg. Lat. | 0 | 5 | 10 | 15 | 20 | 25 | 30 | 35 | 40 | 45 | 50 | 55 | 60 | 65 | 70 | 75 | 80 |
|---|---|---|---|---|---|---|---|---|---|---|---|---|---|---|---|---|---|
| **Northern Hemisphere** | | | | | | | | | | | | | | | | | |
| 1000 Mb. | 17.4 | 16.5 | 16.2 | 15.3 | 13.5 | 12.2 | 10.3 | 9.2 | 7.8 | 6.3 | 5.2 | 4.2 | 3.5 | 2.9 | 2.3 | 2.0 | 1.5 |
| 850 | 11.1 | 11.4 | 10.8 | 9.9 | 8.7 | 7.6 | 6.5 | 5.5 | 4.7 | 4.0 | 3.5 | 3.1 | 2.7 | 2.3 | 2.0 | 1.5 | 1.2 |
| 700 | 6.3 | 6.3 | 5.8 | 5.1 | 4.3 | 3.8 | 3.1 | 2.7 | 2.5 | 2.2 | 2.0 | 1.8 | 1.5 | 1.3 | 1.1 | 1.0 | 0.8 |
| 500 | 1.9 | 2.0 | 1.9 | 1.6 | 1.3 | 1.3 | 1.1 | 0.8 | 0.7 | 0.7 | 0.6 | 0.5 | 0.4 | 0.4 | 0.3 | 0.3 | 0.2 |
| **Southern Hemisphere** | | | | | | | | | | | | | | | | | |
| 1000 Mb. | 17.4 | 16.5 | 15.6 | 13.8 | 11.7 | 10.1 | 8.5 | 7.3 | 6.0 | 4.9 | 3.8 | 2.7 | 1.9 | 1.4 | 1.0 | 0.7 | 0.5 |
| 850 | 11.2 | 11.1 | 10.3 | 9.1 | 7.9 | 6.7 | 5.7 | 4.9 | 4.1 | 3.4 | 2.7 | 2.1 | 1.6 | 1.2 | 0.9 | 0.6 | 0.4 |
| 700 | 6.3 | 6.1 | 5.3 | 5.0 | 4.1 | 3.5 | 2.8 | 2.4 | 2.0 | 1.7 | 1.5 | 1.1 | 0.9 | 0.7 | 0.5 | 0.3 | 0.1 |
| 500 | 2.1 | 2.0 | 2.0 | 1.8 | 1.5 | 1.2 | 1.0 | 0.8 | 0.7 | 0.6 | 0.5 | 0.4 | 0.3 | 0.3 | 0.2 | 0.2 | 0.1 |

Table 3

*Zonally averaged values of the temporal standard deviation of the specific humidity $\sigma(q)$ in gm kg$^{-1}$ for yearly data*

| Deg. Lat. | 0 | 5 | 10 | 15 | 20 | 25 | 30 | 35 | 40 | 45 | 50 | 55 | 60 | 65 | 70 | 75 | 80 |
|---|---|---|---|---|---|---|---|---|---|---|---|---|---|---|---|---|---|
| **Northern Hemisphere** | | | | | | | | | | | | | | | | | |
| 1000 Mb. | 1.4 | 1.6 | 2.0 | 2.4 | 2.7 | 3.2 | 3.3 | 3.3 | 3.1 | 2.7 | 2.4 | 2.4 | 2.3 | 2.3 | 2.0 | 1.9 | 1.8 |
| 850 | 1.7 | 1.9 | 2.3 | 2.6 | 2.8 | 3.0 | 3.1 | 3.1 | 2.8 | 2.5 | 2.2 | 2.0 | 1.9 | 1.8 | 1.6 | 1.4 | 1.6 |
| 700 | 2.1 | 2.3 | 2.6 | 2.7 | 2.7 | 2.6 | 2.5 | 2.3 | 2.0 | 1.8 | 1.6 | 1.4 | 1.3 | 1.1 | 1.0 | 0.8 | 0.7 |
| 500 | 1.5 | 1.4 | 1.4 | 1.4 | 1.3 | 1.2 | 1.1 | 1.0 | 0.8 | 0.7 | 0.6 | 0.6 | 0.5 | 0.4 | 0.3 | 0.3 | 0.2 |
| **Southern Hemisphere** | | | | | | | | | | | | | | | | | |
| 1000 Mb. | 1.5 | 1.8 | 2.3 | 3.0 | 2.9 | 2.9 | 2.7 | 2.4 | 2.1 | 1.9 | 1.6 | 1.3 | 1.1 | 1.0 | 0.8 | 0.7 | 0.5 |
| 850 | 1.9 | 2.2 | 2.6 | 3.0 | 3.1 | 2.9 | 2.6 | 2.2 | 1.9 | 1.6 | 1.2 | 1.0 | 0.8 | 0.7 | 0.5 | 0.4 | 0.3 |
| 700 | 2.0 | 2.3 | 2.6 | 2.7 | 2.5 | 2.2 | 1.8 | 1.5 | 1.3 | 1.2 | 1.0 | 0.8 | 0.6 | 0.5 | 0.4 | 0.3 | 0.7 |
| 500 | 1.4 | 1.3 | 1.1 | 1.0 | 0.9 | 0.8 | 0.6 | 0.6 | 0.6 | 0.5 | 0.4 | 0.3 | 0.2 | 0.2 | 0.1 | 0.1 | 0.1 |

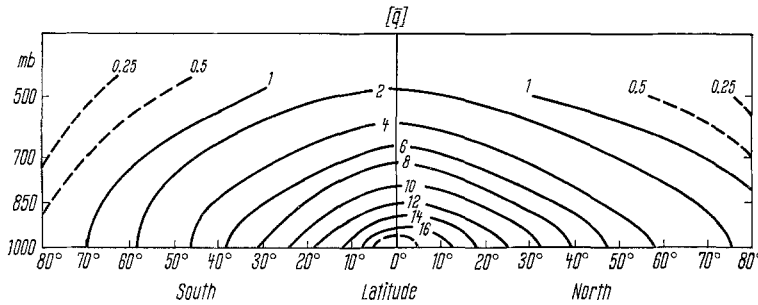


Figure 4
Vertical distribution of zonally averaged values of the specific humidity $\bar{q}$ in units of gm kg$^{-1}$ for yearly data

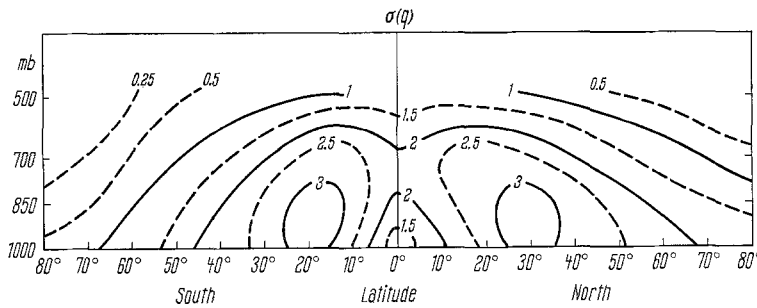


Figure 5
Vertical distribution of zonally averaged values of the temporal standard deviation of the specific humidity $\sigma(q)$ in units of gm kg$^{-1}$ for yearly data

to be expected in view of the intense vertical transport of water vapor from the surface of the oceans associated with the prevailing convection and turbulent diffusion over this region, the largest variability of water vapor as given by (9) in Figure 5 is found in subtropical and middle latitudes in the lower portion of the atmosphere between 1000 and 850 mb, in response to changes of the predominant air masses over these regions.

### *4.2. The zonal flux of water vapor*

The analysis of the field of total zonal transport of water vapor is presented in Figure 5. The outstanding features of the $\bar{Q}_\lambda$ map are consistent with the distribution of the mean zonal flow, i.e., with the mid-latitude westerlies alternating with polar and low latitude easterlies. Contrary to the precipitable water field $\bar{W}$, the analysis of the $\bar{Q}_\lambda$ field shows that the conditions are not zonally uniform and large scale asymmetries are a significant feature of the analyses as revealed by the existence of organized centers with different signs and intensities. Large positive (west to east)

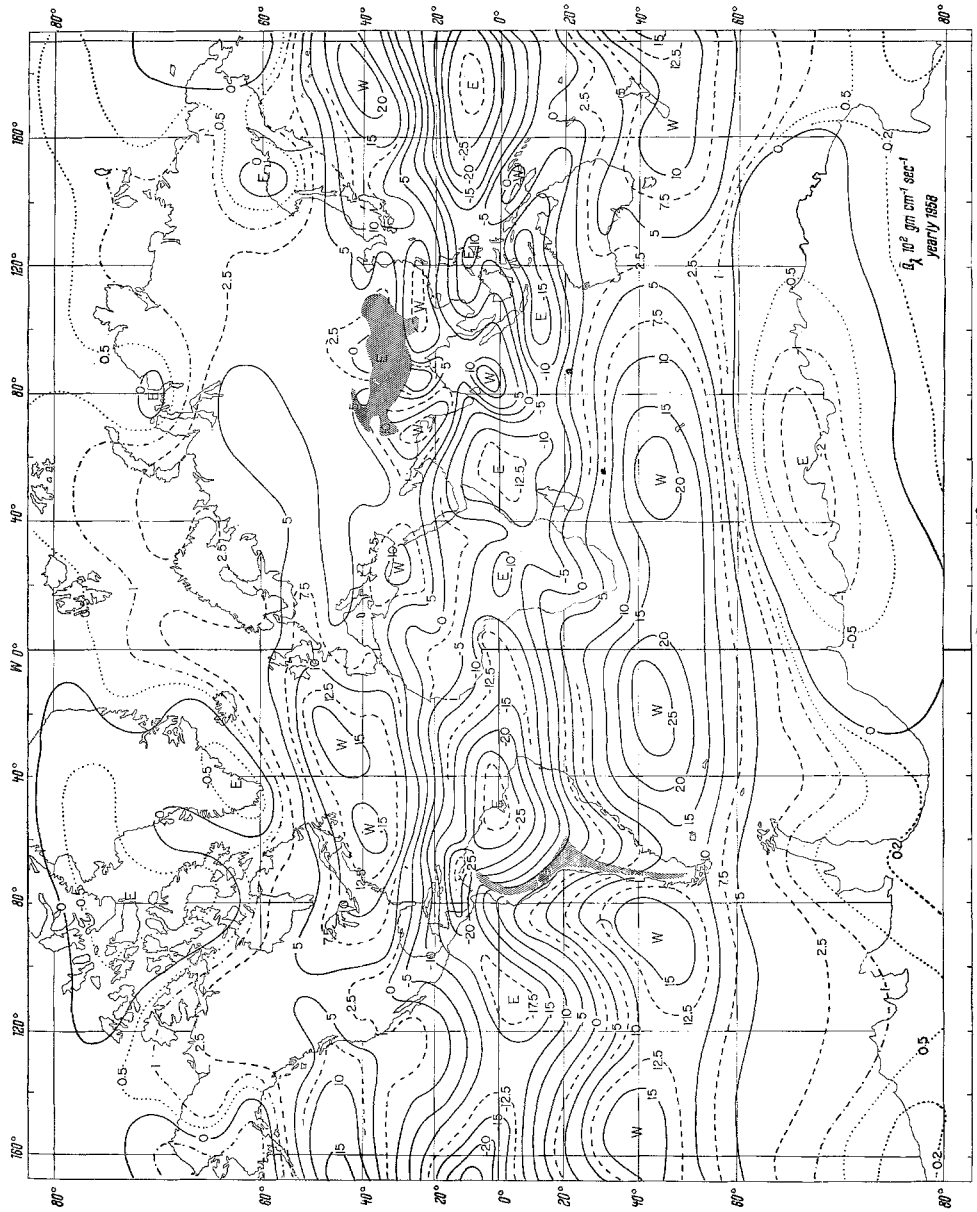


Figure 6. Time average of the vertically integrated zonal transport of water vapor in the atmosphere, $\bar{Q}_\lambda$, in units of $10^2$ gm cm$^{-1}$ sec$^{-1}$, for yearly data. Isoline spacing (full curves) $5 \times 10^2$ gm cm$^{-1}$ sec$^{-1}$

centers of zonal transport are found in both hemispheres in mid-latitudes where westerly winds are predominant, especially over the Pacific, Atlantic and South Indian Oceans. Large negative (east-to-west) centers of zonal transport are found in low latitudes where strong, persistent easterly winds prevail. Two centers of maximum zonal transport are found in the northern part of the equatorial region, one over the North Pacific Ocean near the Marshall Islands and another over the central Atlantic Ocean, extending from Africa to the northern coast of South America and Puerto Rico. A series of small centers of negative zonal transport are also found in the subpolar regions along the southern fringes of the Arctic, over the Sea of Okhotsk, over the Gulf of Ob in north central Siberia and two fairly large and definite negative areas, one over western Alaska and another over the Arctic Archipelago of Canada and Greenland. In the southern hemisphere an extensive and well developed center is found over the Antarctic Coast alternating with regions of positive zonal transport.

The mean zonal values of the zonal flux $[\bar{Q}_\lambda]$, as shown in Figure 7 and given in

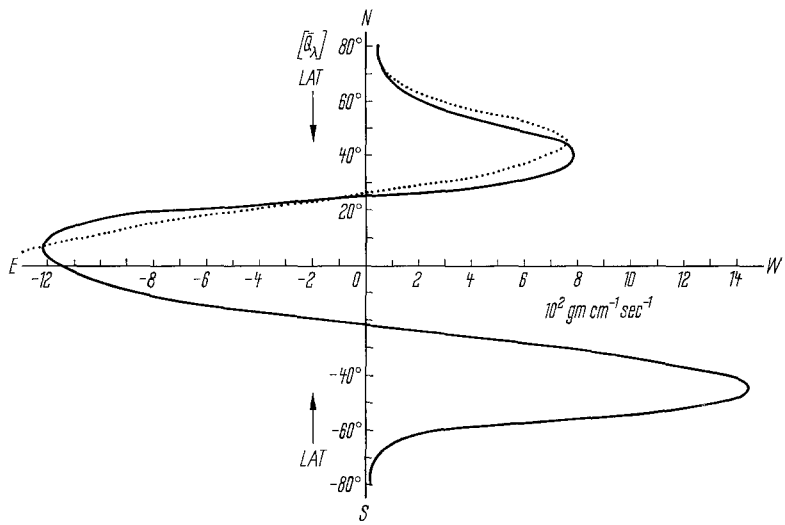


Figure 7

The meridional distribution of the vertical integrated mean zonal flux of water vapor in the atmosphere $[\bar{Q}_\lambda]$ computed from atmospheric data. The dotted curve represents the yearly distribution computed by Starr et al. for 1950. The units are $10^2$ gm cm$^{-1}$ sec$^{-1}$

Table 4, summarize the main characteristics of the zonal flux of water vapor. The largest positive values occur in both hemispheres in the vicinity of 45° latitude, but in the southern hemisphere the flow is much more intense. The change from eastward to westward transport are found at 25°N and 22°S, respectively, in the northern and in the southern hemispheres. Between 25°N and 22°S the mean zonal flow is negative with the highest value to north of the equator. The curve obtained for the year 1950 is also shown for comparison [22].

Table 4

*Zonally averaged values of the mean total zonal flux of water vapor* $[\bar{Q}_\lambda]$, *in units of* $10^2$ *grams per centimeter per second*

| Degrees Latitude | Northern Hemisphere | Southern Hemisphere |
|---|---|---|
| 0 | −11.30 | −11.30 |
| 5 | −12.30 | −10.27 |
| 10 | −12.00 | − 8.72 |
| 15 | −10.11 | − 5.69 |
| 20 | − 5.90 | − 1.29 |
| 25 | 0.14 | 3.31 |
| 30 | 4.79 | 6.88 |
| 35 | 7.18 | 10.44 |
| 40 | 7.98 | 13.45 |
| 45 | 7.42 | 14.51 |
| 50 | 5.85 | 12.71 |
| 55 | 3.59 | 8.48 |
| 60 | 1.98 | 4.11 |
| 65 | 1.34 | 1.61 |
| 70 | 0.80 | 0.50 |
| 75 | 0.46 | 0.14 |
| 80 | 0.11 | 0.20 |

The mean zonal transports of water vapor at various levels, $[\overline{q\,u}]$, are given in Table 5 and in Figure 8. The profile shows two well developed centers of westerly transport at middle latitudes alternating with centers of easterly transport over the subtropical and polar regions. The centers of westerly transport attain their maximum values, in both hemispheres, above the 800 mb level, being more intense over the southern hemisphere. The maximum easterly flux occurs in the northern equatorial region but at a lower level, below 850 mb. The predominant easterly flow over the subpolar and high latitude region are confined to a shallow layer in the lower atmosphere.

The figure also shows that there is an appreciable zonal flux of water vapor at the 500 mb level. As we saw, some studies conducted for individual stations proved that in certain circumstances such flow is still significant above 300 mb and occasionally even above 200 mb. The 'water vapor jet stream' is lower and slightly displaced towards the equator with respect to the mean position of the wind jet stream, which is to be expected in view of the characteristic behavior in the atmosphere of the functions $\bar{u}(p)$ and $\bar{q}(p)$. In fact, the almost linearly increasing values of $\bar{u}$ with height in the mid-latitudes combined with the corresponding almost exponentially decreasing values of $\bar{q}$ with height lead to the formation of the water vapor jet stream in the lower mid-atmosphere, and to a considerable zonal flow of water vapor at the 500 mb or at still higher levels. This shows that the contribution from the levels above 500 mb for the total zonal flux of water vapor is not to be disregarded in the water balance of the atmosphere.

Table 5

*Zonally averaged values of the mean zonal transport of water vapor* $[\bar{F}_\lambda]$, *in units of* $10^{-1}$ *gm (cm mb sec)*$^{-1}$ *for yearly data*

| Deg. Lat. | 1000 mb | 850 | 700 | 500 |
|---|---|---|---|---|
| | | Northern Hemisphere | | |
| 0 | −24.74 | −25.41 | −18.88 | − 7.50 |
| 5 | −22.02 | −31.43 | −22.86 | − 7.55 |
| 10 | −30.51 | −37.04 | −20.31 | − 5.82 |
| 15 | −32.25 | −34.49 | −12.14 | − 3.67 |
| 20 | −25.51 | −20.20 | − 2.65 | − 0.41 |
| 25 | −13.78 | − 3.47 | 7.35 | 4.18 |
| 30 | − 0.20 | 9.59 | 14.08 | 8.06 |
| 35 | 10.00 | 19.59 | 17.55 | 10.10 |
| 40 | 13.16 | 21.53 | 18.57 | 10.20 |
| 45 | 11.43 | 18.67 | 15.71 | 8.37 |
| 50 | 8.16 | 14.08 | 12.45 | 6.33 |
| 55 | 4.49 | 9.80 | 8.06 | 4.59 |
| 60 | 1.12 | 5.82 | 4.80 | 3.16 |
| 65 | − 0.31 | 3.16 | 3.27 | 2.35 |
| 70 | 0.00 | 1.53 | 2.96 | 1.63 |
| 75 | 0.00 | 1.02 | 1.73 | 1.02 |
| 80 | 0.41 | 0.20 | 0.20 | 0.71 |
| | | Southern Hemisphere | | |
| 0 | −24.74 | −25.41 | −18.88 | − 7.50 |
| 5 | −23.57 | −25.10 | −14.39 | − 5.12 |
| 10 | −25.45 | −27.55 | − 9.49 | − 1.49 |
| 15 | −22.52 | −23.98 | − 3.32 | 2.98 |
| 20 | −15.07 | −12.86 | 3.37 | 6.04 |
| 25 | − 4.66 | − 1.33 | 10.41 | 7.85 |
| 30 | 4.77 | 9.18 | 16.12 | 9.45 |
| 35 | 12.85 | 17.86 | 21.73 | 12.01 |
| 40 | 20.86 | 26.33 | 25.82 | 13.76 |
| 45 | 23.30 | 29.29 | 25.97 | 14.10 |
| 50 | 21.51 | 28.16 | 22.14 | 12.05 |
| 55 | 15.84 | 17.45 | 15.23 | 8.22 |
| 60 | 8.86 | 9.39 | 8.82 | 4.93 |
| 65 | 2.09 | 2.65 | 4.78 | 2.17 |
| 70 | − 0.74 | − 0.26 | 2.59 | 1.20 |
| 75 | − 1.73 | − 0.71 | 1.33 | 0.81 |
| 80 | − 0.37 | − 0.08 | 0.72 | 0.59 |

### *4.3. Meridional transport of water vapor*

The analysis of the total mean meridional transport of water vapor, as shown in Figure 9, is not so simple as the corresponding analysis of the mean precipitable water. Large scale asymmetries exist in the global pattern which are averaged out when the

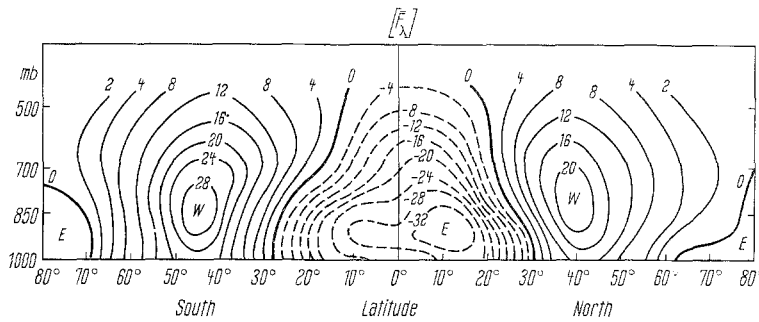


Figure 8
The vertical distribution of mean zonal transport of water vapor in the atmosphere $[\bar{F}_\lambda]$, for yearly data. The units are $10^{-1}$ gm (cm sec mb)$^{-1}$

mean meridional statistics are evaluated. These patterns are undoubtedly related to the main features of the general circulation of the atmosphere and to the physiography of the globe, mainly through the distribution of oceans and continents and the topography. The most intense mean meridional flux of water vapor always occurs over the oceans. There are several centers for both southward and northward transport shown on the map. In general, over the northern hemisphere one expects a net southward transport of water vapor to the east of the semi-permanent high pressure cells and a net northward transport to the west of these cells, due to the anticyclonic wind circulation with reversed meridional transports in the southern hemisphere. In the middle latitudes the polar fronts are also very effective in transporting water vapor from the intertropical region toward the poles. Large centers of southward transport at lower latitudes are found in the northern hemisphere over the eastern Atlantic Ocean, the Arabian Sea and over large areas of the Pacific Ocean. These centers correspond to the eastern sides of the semi-permanent Azores high and winter time African high, while the splitting of the Pacific centers is related to the double cell structure of the North Pacific anticyclone.

The mean annual northward transport of water across the latitude of 25°N occurs in three definite regions: the eastern North Pacific, the North Atlantic including the Gulf of Mexico, and the Bay of Bengal. The configuration of these centers over the Pacific and Atlantic Oceans and the orientation of their axes are an indication that they are related to the migrating cyclones associated with the polar front, whereas the center over eastern Asia and the India Ocean is associated with the Asian Monsoon, which becomes insignificant north of 35°N.

It follows also that the mean poleward transport of water vapor in the middle and high latitudes is accomplished mainly by the transient perturbations associated with the polar front in the Atlantic and Pacific Oceans.

In the southern hemisphere the influence of the homogeneity of the underlaying surface of the globe and the large extent of the oceans is evident. However, the effects of the circulation around the large centers of action over the middle latitude regions

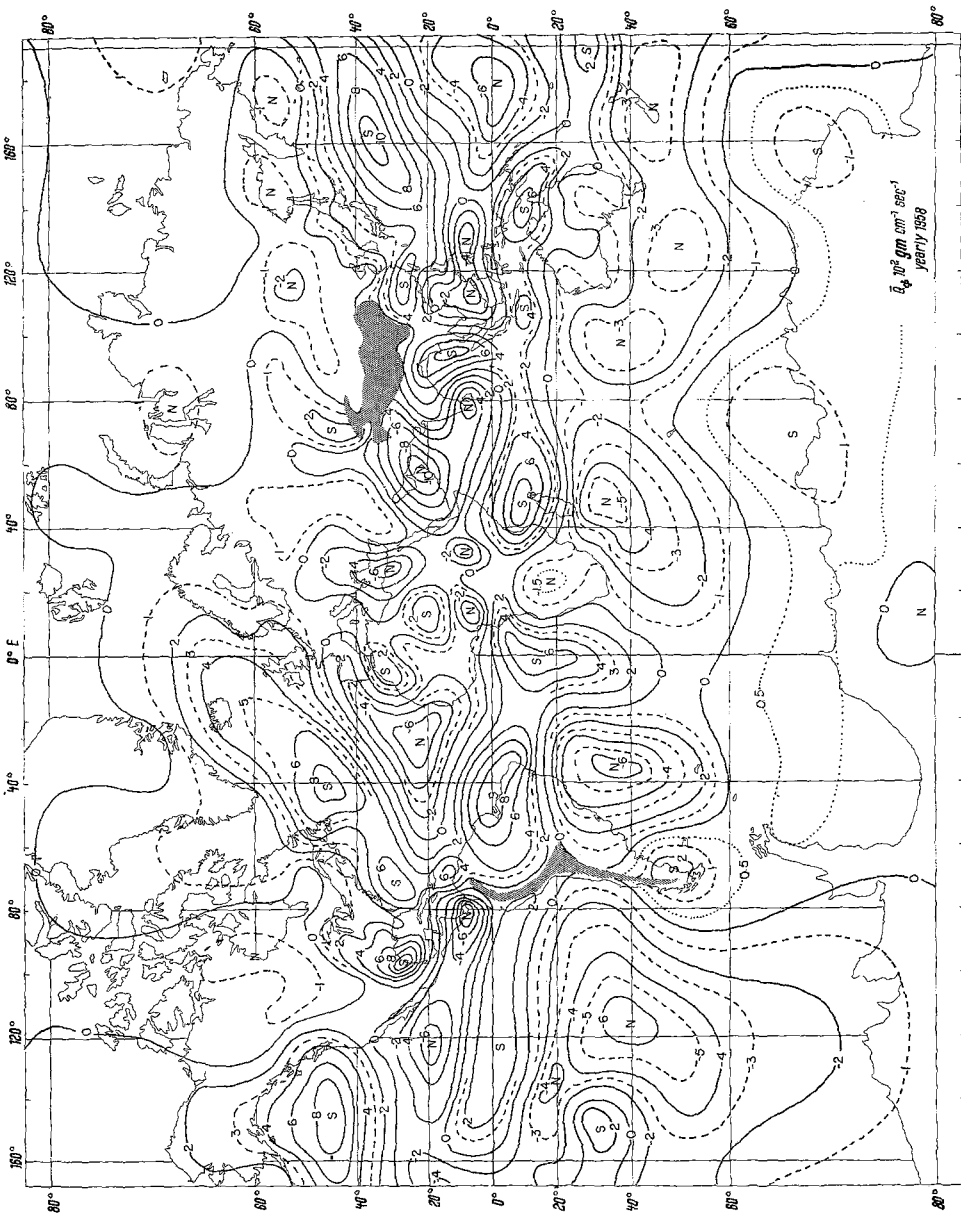


Figure 9. Time average of the vertically integrated meridional transport of water vapor $\bar{Q}_\phi$, in units of $10^2$ grams cm$^{-1}$ sec$^{-1}$ for yearly data. Isoline spacing (full curves) $2 \times 10^2$ gm cm$^{-1}$ sec$^{-1}$

are still indicated by the existence of alternate centers of southward and northward transport of water vapor. These effects are observed over the southern Atlantic Ocean, where a northward transport occurs over Gough Island and southward transports occur over Ilha de Trinidade and over the south coast of Brazil.

In general, the fluxes over the southermost portion of Africa are southward. There is a maximum southward flux over central South Africa. In the middle latitudes the southward flux predominates. Several centers are found south of Australia, over the Indian Ocean south of Madagascar, eastern Atlantic Ocean and over the western Pacific Ocean. Centers of northward transport are found in the Gulf of Guinea and the northern part of South America; over the Central Pacific, over eastern Indian Ocean near Java, and over the Arafura and Coral Seas between Australia and New Guinea, and north of Madagascar. Northward transport centered in middle latitudes are found over the southern part of the South American continent and central Pacific.

For the remainder of the Pacific, however, little can be said due to the scarcity of data. Observations of upper air winds at Rapa indicate that the transport of water vapor there must be northward due to prevailing southerly winds. Accordingly, a center of northward flux has been included there.

Over the high latitudes the meridional flux is predominantly northward and over the continent of Antarctica is very slight everywhere due to the low specific humidity values.

The use of the supplementary intertropical charts improves greatly the analysis over the equatorial region, as is apparent in comparing the actual map with the corresponding analysis for the mean total meridional transport of water vapor presented by PEIXOTO and CRISI [15]. Using the grid point readings from the analysis zonally averaged values of the total meridional transport of water vapor at various latitudes were evaluated. The final values are shown in Figure 10 and in Table 6.

They illustrate in a concise form the main characteristics of the meridional flux

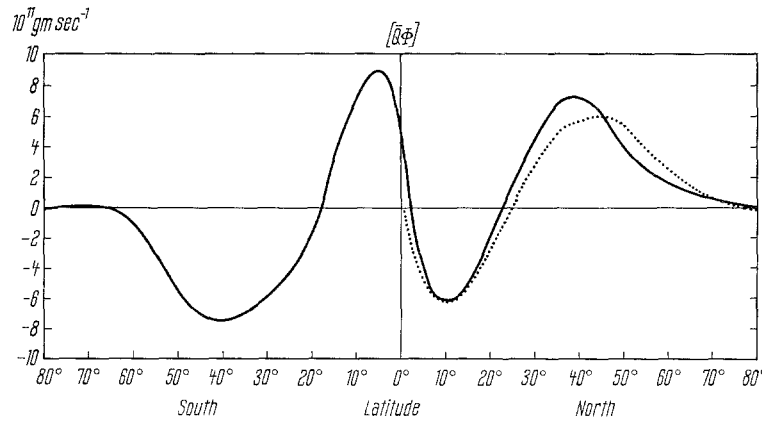


Figure 10

The meridional distribution of the zonally averaged total water vapor transport $[\bar{Q}_\phi]$ across latitude circles in the atmosphere. The dotted curve represents the yearly distribution computed by Starr et al. for 1950. The units are $10^{11}$ gm sec$^{-1}$

Table 6

*Zonally averaged values of the mean total meridional transport of water vapor* $[\bar{Q}_\phi]$ *in units of* $10^{11}$ *grams per second for yearly data*

| Degrees Latitudes | Northern Hemisphere | Southern Hemisphere |
|---|---|---|
| 0 | 4.48 | 4.48 |
| 5 | −4.38 | 8.84 |
| 10 | −6.10 | 7.13 |
| 15 | −5.06 | 3.25 |
| 20 | −1.99 | −1.88 |
| 25 | 1.23 | −4.46 |
| 30 | 4.19 | −5.44 |
| 35 | 6.82 | −6.62 |
| 40 | 7.14 | −7.54 |
| 45 | 6.22 | −7.10 |
| 50 | 4.50 | −5.45 |
| 55 | 2.57 | −3.26 |
| 60 | 1.56 | −1.22 |
| 65 | 1.12 | −0.17 |
| 70 | 0.41 | 0.10 |
| 75 | 0.17 | 0.01 |
| 80 | 0.03 | −0.05 |

of water vapor and summarize many of the details already discussed. In Figure 10 the curve with the yearly distribution computed by STARR, PEIXOTO and LIVIDAS [24] for the year 1950 is also included for comparison. The largest positive values (northward transport) occur in the vicinity of 40°N and 5°S whereas the largest negative values (southward transport) occur in the vicinity of 10°N and 40°S. The actual analysis and the subsequent computations show that there is a substantial northward transport across the equator, needed to supply the required moisture for the intertropical convergence zone, which, on the average, lies somewhat to the north of the equator, in agreement with the findings of PALMEN and VUORELA [12], and VUORELA and TUOMINEN [26]. This result did not appear in our previous study (STARR and PEIXOTO, [23] due to the insufficiency of data in the equatorial region for the calendar year 1950 used in that study. The scarcity of data over the equatorial region led PEIXOTO and CRISI [15] to the same discrepancy in presenting the preliminary results for the northern hemisphere during the IGY (PALMEN, [11]).

The values now obtained agree very well with those published by BUDYKO [3] and by SELLERS [20] derived from independent data using the balance requirements for the water transport in the atmosphere.

### *4.4. The mean zonal water balance*

Following the procedure previously used by the authors (STARR and PEIXOTO, [21]) the mean zonal divergence for various latitudinal belts was evaluated from the values

given in Table 6, using the equation (10). The results obtained agree quite well with those given by PEIXOTO [14] and are shown in Figure 11 and Table 7. For comparison, independent previous estimates of the evaporation minus the precipitation obtained from aerological data and from climatological normals are also included. The inspection of Figure 11 shows immediately that there is: i) convergence ($\overline{E-P}<0$) between 12°N and 8°S associated with the strong excess of precipitation over evaporation observed in the intertropical zone of convergence; ii) convergence ($\overline{E-P}<0$ poleward of 40°N and 40°S up to 75°S in which the excess of precipitation over

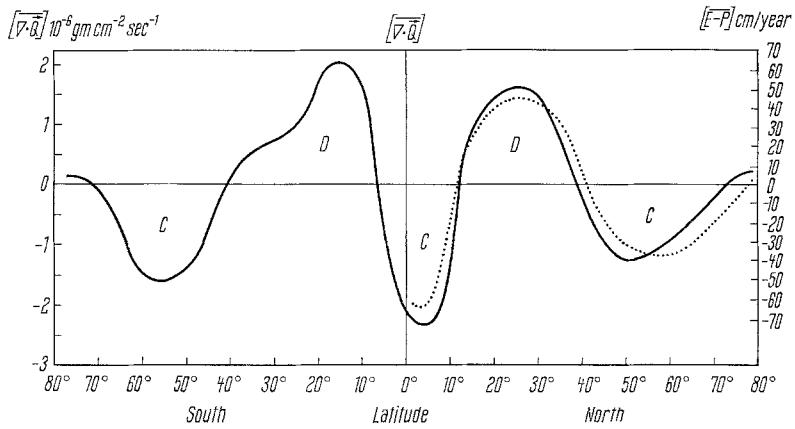


Figure 11

The meridional distribution of the zonally averaged divergence of the water vapor transport $[\overline{\nabla\cdot\vec{Q}}]$. The dotted curve represents the yearly distribution computed by PEIXOTO for 1950. The units are in $10^{-6}$ gm cm$^{-2}$ sec$^{-1}$ and in terms of $\overline{E-P}$ in cm per year

evaporation is associated with the migratory cyclones, the polar front and the alternating air masses; iii) divergence ($\overline{E-P}>0$) over the subtropical regions in both hemispheres where the large semi-permanent anticyclones prevail. Thus, the subtropical regions act as sources of moisture for the atmosphere. The actual values of divergence $\operatorname{div}\overline{\vec{Q}}\sim\overline{E-P}$ agree quite favorably with the values obtained by independent means and compare very well with the previous estimates from the aerological data in the year 1950, (STARR and PEIXOTO [21]) with the exception of the 40–50°N latitudinal belt. The difference might be real since over the region the network was reliable in both studies. However, the discrepancy over the 0–10 belt is due to the improvement of the present analysis.

The vertical structure of the mean total meridional transport can be inferred by analyzing the values of $[\overline{q\ v}]$ given in Table 8 as shown in Figure 12.

The yearly values of $[\overline{q\ v}]$, show that the maximum positive and negative meridional fluxes occur in the lowest part of the atmosphere or even near the surface of the earth. In the lower levels the configuration of the zero isolines which separate the northward from the southward transport shows no indication of return flow aloft up

Table 7

*Meridional distribution of zonally averaged divergence of water vapor flux, $[\overrightarrow{\nabla \cdot Q}]$, in units of $10^{-6}$ gm cm$^{-2}$ sec$^{-1}$; and the difference between precipitation minus evaporation, $\overline{E-P}$, in units of cm year$^{-1}$ by ten degrees latitude belts, as computed from atmospheric data. Independent previous estimates of ($\overline{E-P}$) from aerological data and from climatological normals are also included*

| | 0–10° | 10–20° | 20–30° | 30–40° | 40–50° | 50–60° | 60–70° | 70–80° |
|---|---|---|---|---|---|---|---|---|
| **Northern Hemisphere** | | | | | | | | |
| | − 2.38 | 0.95 | 1.58 | 0.82 | − 0.92 | − 1.12 | − 0.59 | − 0.31 |
| ($\overline{E-P}$) | −75.34 | 30.25 | 48.37 | 25.50 | −26.55 | −36.37 | −19.19 | −10.44 |
| BUDYKO [3] | −69.90 | 23.80 | 45.60 | 13.00 | −26.60 | −32.00 | − 8.20 | − 5.00 (70–90°) |
| STARR and PEIXOTO [21] | −43.30 | 25.10 | 43.30 | 21.80 | − 1.40 | −36.10 | −30.10 | −17.30 |
| PEIXOTO and CRISI [15] | −42.50 | 30.30 | 48.50 | 26.60 | −26.00 | −36.20 | −19.20 | − 8.30 (70–90°) |
| **Southern Hemisphere** | | | | | | | | |
| | − 0.59 | 2.09 | 0.91 | 0.57 | −0. 73 | − 1.61 | − 0.68 | 0.12 |
| ($\overline{E-P}$) | −19.28 | 66.34 | 27.87 | 18.16 | −19.39 | −52.32 | −22.06 | 4.12 |
| BUDYKO [21] | −14.10 | 40.90 | 55.90 | 32.40 | −33.10 | −52.60 | −24.40 | − 3.70 |

Table 8

*Zonally averaged values of the mean meridional transport of water vapor* $[\bar{F}_\phi]$, *in values of* $10^{-1}$ *gm (cm mb sec)*$^{-1}$ *for yearly data*

| Deg. Lat. | 1000 mb | 850 | 700 | 500 |
|---|---|---|---|---|
| | | Northern Hemisphere | | |
| 0 | 13.09 | 5.67 | 0.22 | 0.31 |
| 5 | 3.15 | −1.62 | −1.10 | 0.00 |
| 10 | −6.83 | −1.71 | −0.60 | −0.60 |
| 15 | −7.98 | 1.57 | 1.38 | 1.28 |
| 20 | −7.86 | 3.46 | 3.45 | 1.44 |
| 25 | −3.37 | 4.44 | 3.43 | 1.48 |
| 30 | 0.88 | 4.16 | 3.89 | 1.51 |
| 35 | 5.77 | 5.01 | 3.93 | 1.33 |
| 40 | 6.65 | 5.08 | 3.29 | 1.49 |
| 45 | 6.64 | 4.91 | 2.31 | 0.94 |
| 50 | 3.34 | 3.21 | 1.64 | 0.59 |
| 55 | 1.11 | 1.81 | 1.35 | 0.35 |
| 60 | 0.46 | 1.28 | 1.02 | 0.31 |
| 65 | 0.13 | 0.95 | 0.86 | 0.26 |
| 70 | −0.42 | 0.52 | 0.31 | 0.11 |
| 75 | −0.16 | 0.13 | 0.18 | 0.05 |
| 80 | 0.00 | 0.00 | 0.05 | 0.03 |
| | | Southern Hemisphere | | |
| 0 | 13.09 | 5.67 | 0.22 | 0.31 |
| 5 | 17.15 | 8.58 | 0.66 | 0.05 |
| 10 | 18.25 | 7.26 | 0.01 | −0.64 |
| 15 | 14.69 | 2.42 | −1.53 | −1.20 |
| 20 | 7.84 | −1.49 | −2.53 | −1.15 |
| 25 | 0.67 | −3.82 | −2.98 | −0.69 |
| 30 | −2.61 | −4.67 | −3.01 | −0.44 |
| 35 | −4.05 | −5.30 | −3.47 | −0.38 |
| 40 | −4.76 | −5.33 | −3.58 | −0.74 |
| 45 | −4.36 | −4.68 | −2.77 | −1.08 |
| 50 | −3.17 | −3.59 | −2.13 | −1.08 |
| 55 | −1.23 | −1.59 | −1.35 | −0.87 |
| 60 | 0.25 | −0.58 | −0.72 | −0.53 |
| 65 | 0.93 | −0.27 | −0.42 | −0.27 |
| 70 | 0.89 | −0.19 | −0.22 | −0.09 |
| 75 | 0.31 | −0.10 | −0.12 | −0.02 |
| 80 | 0.21 | −0.02 | −0.08 | −0.01 |

to 500 mb. The relative contribution of the lowest levels for the total meridional transport is now much larger than for the zonal transport, and a large fraction of the meridional transport is confined to the lowest layers of the atmosphere, mainly in the intertropical centers where the influence of the trade winds with a strong meridional component in those layers is decisive. Using the values of $[\overline{q\ v}]$ we computed the mean zonal value of the divergence at various levels shown in Figure 13 and in Table 9,

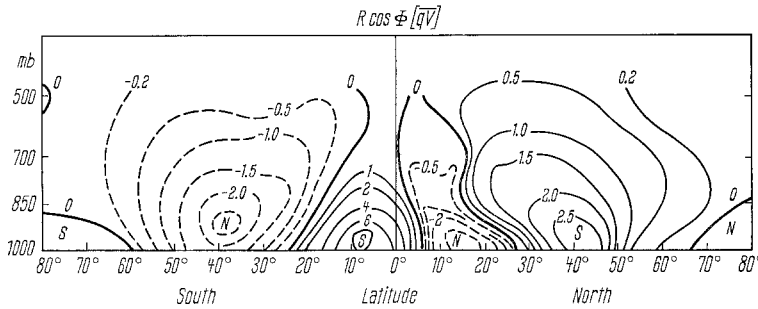


Figure 12
Vertical distribution of zonally averaged values of the meridional transport of water vapor, $2\pi R \cos\phi [\bar{F}_\phi]$ in the atmosphere in units of $10^8$ gm (sec mb)$^{-1}$ for yearly data

in units of $10^{-7}$ gm cm$^{-2}$ sec$^{-1}$ mb$^{-1}$. As was to be expected there are three centers of convergence alternating with two regions of strong divergence. The main center of convergence is localized over the equatorial region, and extends almost to the 500 mb level with most of the convergence occurring in the lower portion of the atmosphere, below 850 mb. The strong convergence is associated with the mean meridional circulation cells. The other centers of convergence are found over the middle latitudes in both hemispheres and are less intense than the equatorial one and are mainly associated with transient cyclones and the polar front.

Centers of divergence are found over subtropical latitudes and are obviously associated with the large belt of anticyclones which are developed mainly over the oceanic area. Although the highest values occur in the lower layers of the atmosphere, they attain relatively considerable values up to 500 mb. There seems to be an indication that two regions of divergence are observed over the subpolar regions, but they extend only within a shallow portion of the atmosphere with small intensities.

Thus the primary and most important sources of moisture for the whole atmosphere are found over the subtropical regions, where the evaporation exceeds by far the observed precipitation. The moisture supplied to the atmosphere over these

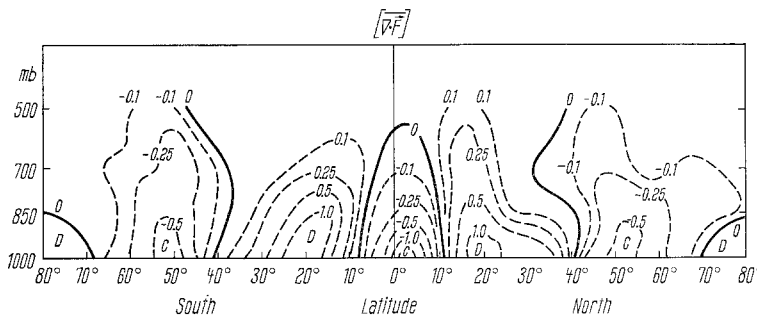


Figure 13
Vertical distribution of zonally averaged values of the mean divergence of water vapor transport $[\nabla \cdot \vec{F}]$ in units of $10^{-7}$ gram cm$^{-2}$ sec$^{-1}$ mb$^{-1}$ for yearly data

Table 9

*Zonally averaged values of the mean zonal divergence of water vapor transport* $[\overline{\nabla \cdot \vec{F}}]$ *in units of* $10^{-7}$ *gram* $cm^{-2}$ $sec^{-1}$ $mb^{-1}$ *for yearly data*

| | Northern Hemisphere | | | | | | | |
|---|---|---|---|---|---|---|---|---|
| | 0–10° | 10–20° | 20–30° | 30–40° | 40–50° | 50–60° | 60–70° | 70–80° |
| 1000 mb | −18.01 | 9.76 | 8.70 | 6.34 | −4.22 | −4.52 | −1.88 | 1.46 |
| 850 | − 6.67 | 4.85 | 0.69 | 0.90 | −2.39 | −3.03 | −1.62 | −1.81 |
| 700 | − 0.74 | 3.80 | 0.43 | −0.66 | −2.10 | −0.97 | −1.31 | −0.91 |
| 500 | 0.26 | 1.91 | 0.07 | 0.33 | −1.15 | −0.44 | −0.43 | −0.28 |
| | Southern Hemisphere | | | | | | | |
| | 0–10° | 10–20° | 20–30° | 30–40° | 40–50° | 50–60° | 60–70° | 70–80° |
| 1000 mb | −4.66 | 9.76 | 10.39 | 2.36 | −2.02 | −4.58 | −1.36 | 2.37 |
| 850 | −1.44 | 8.21 | 3.16 | 0.83 | −2.12 | −4.72 | −0.83 | −0.59 |
| 700 | 0.19 | 2.38 | 0.48 | 0.62 | −1.86 | −2.21 | −1.07 | −0.49 |
| 500 | 0.86 | 0.38 | 0.71 | 0.33 | 0.43 | −2.28 | −0.94 | −0.28 |

regions is afterwards transported to other regions where convergence prevails. Therefore, as was previously discussed by the authors (STARR and PEIXOTO [23]) and by LUFKIN [9] the theory of formation of precipitation from evaporation *in situ* cannot be accepted.

### 5. *Concluding Remarks*

With the possible exception of a portion of the Pacific Ocean and the polar regions, it is felt that the present research reliably reflects humidity conditions over the globe during 1958 in a general fashion. It is hoped that the results given offer added insight into these conditions and will help to provide the basis for further intensive studies. Certainly the possibilities for further research are plentiful.

The excellent agreement of the actual results with those obtained by the authors for the northern hemisphere in previous studies seems to secure the consistency of the approach followed and of the methodology utilized. Thus, it is reasonable to expect that in extending to the southern hemisphere the same methodology, the results obtained will depict the most prominent characteristics of the flow of the water vapor. However, it is assumed that with the desirable improvement of the southern hemispheric network and the implementation of new instrumental techniques much can be done to improve the actual results.

The present work points to the necessity of extending this type of study to longer periods of time and to a larger number of isobaric levels mainly in the lower layers of the atmosphere where the moisture flux is dominant. It seems that a 50 mb resolution in the vertical would be the minimum for truly adequate studies of the moisture flux and of the water balance. In fact, the present paper must be regarded only as a pilot study for further developments in this field like those already in progress at the M.I.T. Planetary Circulations Project under the auspices of the National Science Foundation.

### *Acknowledgments*

This research was supported by the Atmospheric Sciences Section, National Science Foundation, NSF Grant GA-1310X. The cooperation of the United States Air Force in providing and processing the basic IGY data for the Northern Hemisphere is acknowledged. Most of the subsequent computations for this study were carried out by the M.I.T. Computation Center on an I.B.M. 7094 digital computer.

Thanks are due to Miss JUDY ROXBOROUGH for aiding with the preparation of the data and with the computations; to Miss ISABEL KOLE for reading the maps and drafting the figures, and to MRS. MARIE L. GABBE for typing the manuscript.

### REFERENCES

[1] J. K. BANNON and L. P. STEELE, *Average water vapour content of air*, Met. Office, Geophysical Memoir No. 102 (1960), 38.

[2] G. S. BENTON and M. A. ESTOQUE, *Water vapor transfer over the North American Continent*, J. Meteor. 11 (1954) 462.
[3] M. I. BUDYKO, *Atlas teplovogo balansa Zemnogo Shara*, U.S.S.R. Glavnaia geofizicheskaia observatoriia (1963), 69. (Text translated by Irene A. Donchoo as Guide to the Atlas of the heat balance of the earth; distributed by U.S. Weather Bureau, Washington, D.C.)
[4] A. S. GRIGOR'EVA, *The transport of water vapour over the European territory of the U.S.S.R. in different months* (in Russian), Glav. geofys. Obs., Leningrad, Trudy, Vyp. *89* (1959), 3.
[5] A. S. GRIGOR'EVA, *The transport of water vapour over the middle latitudes of Eurasia* (in Russian), Ibid. *111* (1961), 24.
[6] A. S. GRIGOR'EVA, *Fluxes of water vapour in G. Ya. Vangengeim's atmospheric circulation types* (in Russian) Ibid. *111* (1961), 37.
[7] J. W. HUTCHINGS, *Water-vapor transfer over the Australian Continent*, J. Meteor. *18* (1961), 615.
[8] E. N. LORENZ, *The nature and theory of the general circulation of the atmosphere*, World Meteorological Organization (1967), 169.
[9] D. LUFKIN, *Atmospheric water vapor divergence and the water balance at the earth's surface*, Sci. Rpt. 4, General Circulations Project, Mass. Inst. of Tech. (1959), 44.
[10] A. NYBERG, *A determination of some monthly values of evapotranspiration in Finland and in a region in the North-Eastern Atlantic*, Geophysica 6 (1958), 377.
[11] E. PALMÉN, *Evaluation of atmospheric moisture transport for hydrological purposes*, World Meteorological Organization, Reports on WMO/IHD, Geneva (1967).
[12] E. PALMÉN and L. A. VUORELA, *On the mean meridional circulations in the northern hemisphere during the winter season*, Quart. J. Roy. Met. Soc. *89* (1963), 131.
[13] J. P. PEIXOTO, *Hemispheric humidity conditions during the year 1950*, Sci. Rep. 3, General Circulations Project, Mass. Inst. of Tech. (1958), 142.
[14] J. P. PEIXOTO, *On the global water vapor balance and the hydrological cycle*, Tropical Meteorology in Africa, Munitalp Foundation, Nairobi (1960), 446.
[15] J. P. PEIXOTO and A. R. CRISI, *Hemispheric humidity conditions during the IGY*, Sci. Report No. 6, Planetary Circulations Project, Mass. Inst. of Tech. (1965), 166.
[16] J. P. PEIXOTO and G. O. P. OBASI, *Humidity conditions over Africa during the IGY*, Sci. Report No. 7, Planetary Circulations Project, Mass. Inst. of Tech. (1965), 143.
[17] E. M. RASMUSSON, *Atmospheric water vapor transport and the hydrology of North America*, Report No. A-1, Planetary Circulations Project, Mass. Inst. of Tech. (1966), 170.
[18] E. M. RASMUSSON, *Diurnal variations in the summer water vapor transport over North America*, Wat. Resources Research *2* (1966), 469.
[19] E. M. RASMUSSON, *Atmospheric water vapor transport and the water balance of North America*, Mon. Wea. Rev. *95* (1967), 403.
[20] W. D. SELLERS, *Physical Climatology* (University of Chicago Press, Chicago 1965), 272.
[21] V. P. STARR and J. P. PEIXOTO, *On the global balance of water vapor and the hydrology of deserts*, Tellus *10* (1958), 189.
[22] V. P. STARR and J. P. PEIXOTO, *On the zonal flux of water vapor in the Northern Hemisphere*, Geof. pura e appl. *47* (1960), 199.
[23] V. P. STARR and J. P. PEIXOTO, *The hemispheric eddy flux of water vapor and its implications for the mechanics of the general circulation*, Arch. f. Met., Geoph. u. Biokl. *14* (1964), 111.
[24] V. P. STARR, J. P. PEIXOTO and G. C. LIVADAS, *On the meridional flux of water vapor in the northern hemisphere*, Geof. pura e appl. *39* (1958), 174.
[25] V. P. STARR and R. M. WHITE, *Direct measurement of the hemispheric poleward flux of water vapor*, Journal of Marine Research *14* (1955), 217.
[26] L. A. VUORELA and I. TUOMINEN, *On the mean zonal and meridional circulations and the flux of moisture in the northern hemisphere during the summer season*, Geof. pura e appl. *57* (1964), 167.
[27] Weather Bureau, Republic of South Africa: World Weather Maps for Southern Hemisphere, International Geophysical Year.
[28] World Weather Maps (IGY): Tropical Zone (25°N–25°S), Deutscher Wetterdienst.

(Received 23rd September 1968)